Journal of Applied Fluid Mechanics, Vol. 13, No. 3, pp. 827-837, 2020.
Available online at www.jafmonline.net, ISSN 1735-3572, EISSN 1735-3645.
DOI: 10.29252/jafm.13.03.30345

The Effect of Swirling Air-to-Liquid Momentum Ratio on the Spray and Droplet Characteristics

M. Chinnaraj and R. Sadanandan†

Department of Aerospace Engineering, Indian Institute of Space Science and Technology (IIST), Thiruvananthapuram, Kerala, India - 695 547

†*Corresponding Author Email: rajeshsadanandan@iist.ac.in*

(Received April 4, 2019; accepted August 25, 2019)

ABSTRACT

The effect of swirl flow on the spray characteristics (structure, droplet diameter and droplet velocity) is experimentally investigated for varying air-to-liquid momentum ratios in this work. The diagnostic techniques employed include high-speed shadowgraphy and 1D-PDPA. A commercial pressure swirl injector is mounted in a swirl stabilized model gas turbine burner to investigate the spray characteristics with and without the presence of swirling flowfield under isothermal conditions. In the absence of the injector flow the burner produced a converging-diverging flowfield at the burner exit, influenced by the bluffbody effect near to the exit and the swirling intensity farther downstream. The investigations reveal an unmistakable influence of the swirling flow on the droplet size, velocity and spatial distribution. Under the investigated momentum flux ratios the conical spray structure is altered and the droplets size and velocity at each location changed with the spatial variation in the magnitude and nature of the swirling flowfield. In general fine droplets are produced near to the high velocity air inflow, and coarser droplets in the recirculation zone owing to the longer residence time. The mean axial velocity of the droplet reduced in presence of swirling flow, with the droplets showing negative velocities at downstream locations.

Keywords: Swirl flow; Sprays; SMD; High-Speed shadowgraphy; PDPA.

NOMENCLATURE

A_a	air flow outlet area
A_l	liquid flow outlet area CTRZ central toroidal recirculation zone
d_l	injector exit diameter
D_{sw}	swirler outer diameter
D_{hub}	swirler hub diameter
D_h	hydraulic diameter
GT	Gas Turbine
KH	Kelvin-Helmholtz
L_s	jet spread
L_l	end point based breakup length
L_p	profile based breakup length
MR	air-to-liquid momentum ratio
PDPA	Phase Doppler Particle Analyser
PIV	Particle Image Velocimetry
Q_a	air flow rate
Q_l	liquid flow rate
r	radial coordinate
Re_{air}	air Reynolds number
SMD	Sauter mean diameter
S	Swirl number
v_a	mean air velocity
v_l	mean liquid velocity
v	mean axial velocity
v_{max}	maximum streamwise velocity
We	Weber number
x	axial coordinate
φ_{glob}	global equivalence ratio
θ	swirler angle
ρ_a	density of air
ρ_l	density of liquid

1. INTRODUCTION

An understanding of the liquid sheet break up and spray formation is fundamental to two-phase flow combustion and propulsion studies as the knowledge gained is vital for improving the combustor performance, efficiency and minimizing pollutant emission levels (Rink & Lefebvre, 1986). Unless the

liquid fuels are well atomized into a large number of fine droplets with uniform distribution and with increased surface area, they will not be volatile enough to produce required vapour for ignition and combustion (Marchione *et al*. 2007). Poor atomization results in bad mixing, degraded ignition performance and increased pollutant emission. Whereas, good atomization results in better mixing of fuel and air, faster rate of fuel evaporation, which results in better combustion and better emission control (Glassman & Yetter, 2008). The in-formation is also indispensable for the development of numerical models that can assist the designers of aero-propulsion engines, gas turbine (GT) burners, domestic and industrial burners, rocket injectors etc (Faeth, 1983).

One of the most commonly used methods for atomization of liquid fuel in practical combustors is utilizing a co-flowing, high-speed gas jet. Under such cases the transfer of kinetic energy from the high-speed swirling gas to the liquid assist in the breakup of the jet, a process known as air-blast atomization when air is the atomizing gas (Lefebvre, 1989). Though it is of considerable practical interest in practical combustion systems as well as being a fundamental research topic in multiphase flow the fundamental aerodynamic and hydrodynamic processes involved in the jet and sheet disintegration into fine droplets are not well understood. In case of atomizers used in aero-propulsion or GT engines the liquid sheet and the droplets are also subjected to flowfields of swirling nature. This is because swirl is predominantly used as a flame stabilizing mechanism in GT engines and also been used for controlling the efficiency and for pollutant reduction (Lefebvre, 1998). A lack of under-standing exists on the effect of swirling gas environment on the atomization process (Wang & Lefebvre, 1987; Rizk & Lefebvre, 1985; Yao *et al*. 2012; Fan *et al*. 2014). This is due to the inherent complexity associated with the liquid atomization process coupled to a gaseous phase with spatially varying velocity and turbulence levels. Even in case of quiescent air, the velocity adjacent to spray can have high velocities due to the high momentum imparted by the spray into the surrounding gas. Also the turbulent nature of the swirling co-flow can influence atomization/droplet characteristics and not many systematic studies have been conducted so far in this regard. For example the experimental studies conducted by Rosa *et al*. on the dynamic behaviour of liquid spray under varying swirl intensities show that the spatial distribution of droplet sizes, velocities, and number density are strongly affected by the swirl flow dynamics (de la Rosa, 1992). Depending on the injector operating conditions, the liquid jet can be subjected to different kinds of instabilities including Kelvin-Helmholtz (KH) instability, Rayleigh-Taylor (RT) instability, helical, etc (Charalampous *et al*. 2019; Kumar & Sahu, 2018; Matas *et al*. 2018; Varga *et al*. 2003). The axial and azimuthal velocity components present in swirling flow will result in the development of KH instability in both axial and azimuthal shear layer leading to the generation of topological structures completely different from those of non-swirling jets (Rajamanickam & Basu, 2017). The swirling flow can even have stabilization or destabilization effect on liquid jet breakup (Lian & Lin, 1990, Liao *et al*. 2000).

In practical swirl combustion systems the droplet diameter is of primary interest. Understanding the dynamic interaction of the swirling gaseous phase with the liquid droplets is intimately related to our understanding of the combustor performance. As local fuel concentration or equivalence ratio, sooting characteristics and pollutant emissions are directly related to the local droplet evaporation rate, information about the spatial distribution of the fuel drop sizes and their velocities in response to the local airflow pattern in the combustion zone is important. Depending on the size of the droplets the droplets may avoid high centrifuging due to swirl, and be affected by the turbulent characteristics of the gas flow (Hadef & Lenze, 2005). This implies that under identical operating conditions of the burner the fuel air mixing characteristics will be different for spray flames and gaseous fuel flames. Therefore information about the droplet distribution and characteristics is also essential in the design and development of these burners using liquid fuels. Atomization, and especially air-blast atomization, is a complex multi-parameter problem. The droplet size, usually defined by the Sauter Mean Diameter (SMD), which is the volume/surface ratio of the spray ($D_{32} = \Sigma Nidi^3/\Sigma Nidi^2$) is dependent on the gas velocity by a power-law $D_{32} \approx U_g^{-n}$ with n ranging usually from 0.8 to 2 (Lasheras *et al*. 1998; Varga *et al*. 2003). Experimental evidence re-veal a two-stage instability mechanism, a primary shear instability followed by a RT instability of the liquid tongues produced by the primary instability (Aliseda *et al*. 2008). The instability in the nearfield originates in the vorticity sheet of the liquid jet and results indicate that the airstream has no influence on the instability. When perturbations are amplified in the downstream locations the aerodynamic form drag on the aerodynamic form drag on the liquid become dynamic and the air stream impels to further destabilization of the liquid jet. The gas stream in the near field can have an appreciable effect on the liquid jet if the gas momentum flux per unit volume is greater than or equal to the liquid jet momentum flux per unit volume. This implies that besides surface tension the air-to-liquid momentum ratio is an important parameter to be considered in atomization of liquid jet surrounded by high-speed gas jets. In this paper, we report an experimental study on the effect of swirling air-to-liquid momentum ratio on the spray and droplet characteristics. The reader is reminded that the present studies are not aimed at investigating the interaction of liquid spray with swirling co-flow under realistic GT/aero-propulsion conditions (high pressure, high temperature and high Reynolds number reactive flows). Instead, the goal here is to get a fundamental level understanding of the influence of swirling co-flow on the droplet characteristics with varying air-to-liquid momentum ratios. The experimental investigations are performed in an in-situ developed and swirl stabilized burner mounted with a commercial pressure swirl injector using water used as a surrogate fuel instead of kerosene. High-speed

Shadowgraphy and Phase Doppler Particle Analyser (PDPA) is used to visualize the spray pattern and to quantify droplet characteristics respectively.

2. EXPERIMENTAL SET-UP

The experimental setup consists of a compressed air supply system, a pressurized (pressurized with compressed air) liquid fuel supply system and a swirl stabilized burner with a commercial injector. Air from the compressor is regulated using a Coriolis flowmeter (model: Micromotion Coriolis elite sensor). The Coriolis flowmeter has a factory calibration specifying accuracy of typically within 0.35% of the mass flow. An in-situ developed swirl stabilized burner for gaseous fuel applications (IIST-GS1) (Jarpala *et al*. 2017) is modified to incorporate the liquid injector for the present investigations. Systematic tests are conducted to in-vestigate the influence of swirl on spray patterns and droplet characteristics at varying air and liquid flow rates mimicking the equivalence ratio variations (based on mass flow rates of fuel and air) present in the liquid combustors.

2.1 Burner and Injector Details

Figure 1 shows the schematic of IIST-GS1 swirl burner incorporated with the commercial fuel injector. More details of the burner can be found elsewhere (Sadanandan, 2015) and only a brief description is given here. The swirling motion is imposed on the main air-flow by means of a radial swirler consisting of 12 vanes and with a swirl angle of 72 degrees. The outer diameter of a radial swirler is 60 mm and the hub diameter is 50 mm. The geometrical swirl number, S, is 2.81, calculated following the expression derived by Beer and Chigier (Lefebvre, 1998),

$$S = \frac{2}{3}\left[\frac{1-\left(\frac{D_{hub}}{D_{sw}}\right)^3}{1-\left(\frac{D_{hub}}{D_{sw}}\right)^2}\right]\tan\theta \qquad (1)$$

Where, D_{sw} and D_{hub} are the outer diameter and hub diameter of the swirler and θ is the swirl angle. The annular space at the burner exit (air nozzle) has outer and inner diameters of 42 and 36 mm respectively, resulting in a hydraulic diameter (D_h) of 6 mm at the nozzle exit. The central region of the bluffbody is recessed in the shape of an inverted truncated cone and the recess height is approximately 11 mm. Care has been taken in the mounting of the injector such that the spray coming out of the injector does not come into contact with the inner walls of the bluffbody.

A commercial pressure swirl injector from Spraytech (Model: SPRAYTECH.HC-9/16-60- 0.025-7-04) is used for the present studies. The pressure swirl atomizer or simplex atomizer are known to have good atomization performance and high combustion stability (Lefebvre, 1989). Here the liquid is discharged under high pressure through a small orifice and atomization is achieved by the conversion of pressure energy into kinetic energy and thereby producing a high relative velocity between the liquid and the surrounding gas. The injector consists of a swirling element near to the injector exit (exit hole diameter 0.3 mm) and has a manufacturer specified cone angle of 60 degrees at an operating pressure of 7 bar. The swirling motion is imparted to the liquid as it discharges out of the orifice and an annular liquid sheet spreading radially (hollow cone) outward is formed due to the centrifugal force. The instabilities (Kelvin-Helmholtz instability) propagating within the thin liquid sheet as well as on the liquid surface will bring about liquid sheet breakup into ligaments and then to droplets. Further disintegration into finer droplets results due to the collision between droplets and the impact of aerodynamic forces. The injector is designed for a factory calibrated maximum liquid flow rate of 0.025 lpm with water.

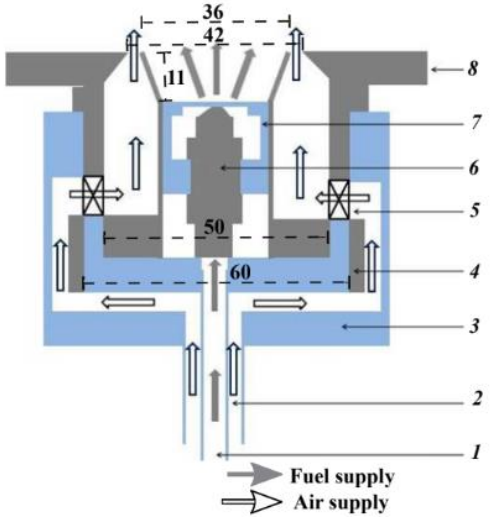

Fig. 1. Schematic of IIST-GS1 incorporated with the commercial injector (1)fuel injection tube,(2)air injection tube, (3) air plenum, (4) threaded sleeve, (5) swirler, (6) fuel injector, (7) injector cover block, (8) air nozzle body; All dimensions in mm.

2.2 Test Conditions

Two non-dimensional numbers are used to characterize the flow, viz., air Reynolds number (Re_{air}) based on the hydraulic diameter of the air nozzle exit D_h and air to liquid momentum ratio (MR). Here air momentum is defined as $\rho_a v^2_a A_a$ and liquid momentum as $\rho_l v_l^2 A_l$, where ρ_a, ρ_l are densities, v_a, v_l the mean velocities and A_a, A_l the outlet flow areas of air and liquid flow respectively. MR therefore represents the interaction of the swirling flowfield on the atomization. For a constant liquid flow rate through the injector, the co-flow air flow rate is varied to impose a variation in the relative momentum of the coflowing air. The spray characterization is done with water as surrogate fuel at an injection pressure of 6 bar to mimick kerosene in reactive test cases. The air and the liquid flow rates corresponding to the different MR investigated are tabulated in Table 1. Here the air and water flowrates arrived at so as to represent a specific global equivalence ratio (based on the mass flow rate of fuel and air) in the reactive flow test cases. For example,

the water flow rate of 0.025 slpm (v_l = 5.9 m/s) through the injector equates to a density corrected flow rate of 0.0276 slpm with kerosene in reactive test cases. So, for a fixed kerosene flow rate of 0.276 slpm the mass flow rate of air shown in Table 1 will there-fore represent three different global equivalence ratios - φ_{glob} = 0.9, 0.7 and 0.5 - with kerosene and air. With kerosene as fuel through the injector the fuel jet velocity will increase in reactive cases, but the momentum flux ratios will remain the same as in the present tests with water.

Another important dimensionless parameter used for correlating the drop size data is the Weber number (W_e), defined as the ratio of the inertial force to the surface tension force, given by:

$$W_e = \frac{\rho_a d_l (v_l - v_a)^2}{\sigma} \quad (2)$$

Table1 Investigated test conditions

Q_a slpm	v_a/v_l	Q_l slpm	Re_{air}	MR
-	-	0.025	-	-
308.4	2.36	0.025	5140.9	35.8
396.5	3.03	0.025	6610.9	59.2
555.1	4.27	0.025	9254.5	116.1

In Weber number space the operating conditions correspond to $W_e \leq 1$ for MR ≤ 59.2 and W_e = 1.89 for MR = 116.1.

3. MEASUREMENT TECHNIQUES

Optical and laser diagnostics methods are employed to examine the spray characteristics and its interaction with the swirling airflow around it. High-speed shadowgraphy is employed to capture the time-resolved spray pattern, and to calculate the spray cone angle and breakup length. A Phase Doppler Particle Analyser (PDPA) is used to quantify the size droplet size and velocities with and without the co-flowing swirling field.

3.1 High-Speed Shadowgraphy

High-speed shadowgraphy technique is employed for the measurement of spray cone angle and breakup lengths. The experimental setup is shown schematically in Fig 2(a). The spray is illuminated using a high-power LED light source, the beams of which are made parallel using a plano-convex lens to get uniformity in the background light of the shadowgraph. It is followed by the injector and a high-speed CMOS camera (model: Phantom V1210) equipped with a long-distance microscopic lens (make: Lavision). The camera array size of 1280 x 800 pixels is used for the measurements at an acquisition rate of 6 kHz. The camera exposure time is set to 4.5 µs for injector tests with-out swirling co-flow, and at 6 µs for tests with the co-swirled airflow.

An automated image processing procedure is followed to obtain instantaneous and time-averaged spray cone-angle, jet spread (L_s) and spray breakup lengths from the high-speed shadowgraph photos (Mohammed *et al*. 2019) (see Fig. 3). Two types of breakup lengths - (i) linear distance from the nozzle exit till the first point of breakup (L_l) and (ii) summation of the incremental length (d_l), by tracking the spray edge profile (L_p)- are estimated (Rajamanickam & Basu, 2017). Around 1650 images are taken to build the time-averaged statistics.

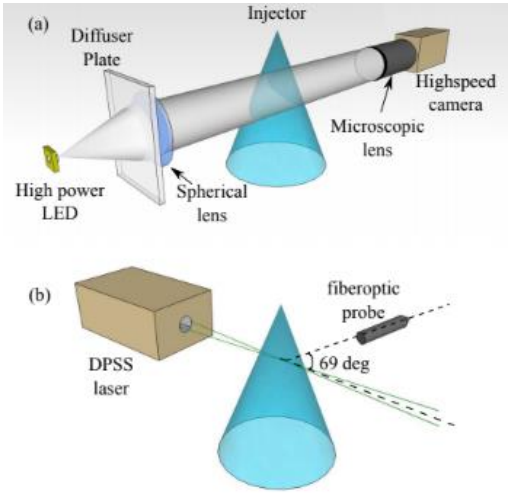

Fig. 2. Schematic of the diagnostic setup used for (a) high-speed shadowgraphy and (b) 1D-PDPA technique.

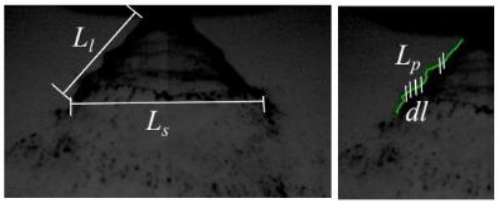

Fig. 3. Definition of spray parameters.

3.2 PDPA Measurements

The fineness of an atomization process is usually defined in terms of mean drop size. The most widely used definition of mean drop size is the Sauter mean diameter (SMD), which is the volume/surface ratio of the spray. A one dimensional PDPA system from TSI (USA) operating in forward-scatter mode (at 69 and 58 degrees off-axis angle for without and with swirling co-flow, respectively) is used for the droplet sizing (SMD) and velocity measurements. Figure 2(b) shows the experimental setup for PDPA measurements. A diode-pumped solid-state (DPSS) laser at λ=532 nm is used for the experimental study. The transmitting optics have a focal length of 350 mm and the receiving optics have a focal length of 300 mm. With a beam separation distance of 50 mm, beam diameter of 2.10 mm, and a receiver slit aperture of 150 µm the fringe spacing is 3.8 µm. The length of the measurement volume is 1700.42 µm. The droplet sizes and the droplet velocities are acquired at 6 cross-sectional planes downstream of the burner exit (z = 0 is referred to as the base of the co-swirled air exit) at z = 5, 10, 15, 25, 35, 50 mm. Also at each cross-sectional plane, data is acquired at off-axis locations in the radial direction of the spray in steps of 5 mm from -25 mm to +25 mm. The

measurement locations and the origin definition are detailed in Fig. 4. The injector is placed in a micrometer traverse to ensure its accurate movement in the axial and radial directions.

For measurements without swirling co-flow 40,000 droplets are measured at a particular location to compute the mean velocity and mean diameter. The data acquisition settings of PDPA system will enable droplet measurements in the velocity range from -15.47 m/s to +19.34 m/s and diameter ranges from 0.50 µm to 149.77 µm. The maximum measured value of velocity and diameter are 5.13 m/s and 29.71 µm respectively. So, the worst-case uncertainty in velocity measurements is ±0.64 % and±3.04 % for diameter. For the tests with co-swirled airflow the droplet count is fixed at 15,000. The velocity ranges that can be measured are from -30.94 m/s to +38.67 m/s. The maximum measured velocity and diameter, in this case, are 18.91 m/s and 45.26 µm respectively. So, the maximum expected uncertainty in velocity and diameter measurements are ±0.46 % and ±2.17 % respectively.

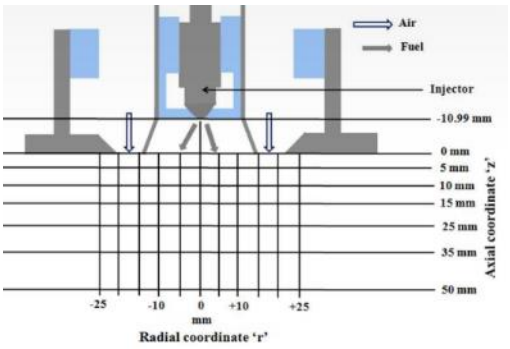

Fig. 4. Injector position and PDPA measurement locations for tests with and without swirling co-flow.

4. RESULTS AND DISCUSSIONS

The results from the high-speed shadowgraphy and PDPA measurements are discussed in detail in the following sections. The results from the non-swirling test cases are compared with selected cases of varying MR to ascertain the impact of swirling flowfield on the droplet distribution and characteristics.

4.1 Spray Cone angle and Spray Pattern Studies

4.11 Without Co-Swirling Air flow

The droplet characteristics downstream of the injection depend on the primary and secondary atomization processes. Figure 5 shows representative instantaneous high-speed shadowgraph images of the spray without any co-swirled airflow. Due to the highly turbulent nature of the flowfield and as atomization is inherently an unsteady process the spray cone angle and the breakup length (L=0 is at the tip of the injector) are varying instantaneously with time. The time-averaged effective cone angle and the jet spread (L_s) is found to be 90.1±13.7 degrees and 5.6±0.9 mm respectively. The endpoint-based (L_l) and profile-based (L_p) breakup lengths measured are 2.7±0.8 mm and 2.8±1.0 mm respectively. A good impression of the variation in the spray parameters is obtained from the histogram, which is shown in Fig. 6. In the case of reactive flows these temporal fluctuations will result in a temporal variation in the local mixture fraction. Also, it should be mentioned that the measured spray cone angle is higher than the manufacturer specified value as the operating pressures are different.

4.12 With Co-Swirling Airflow

A good impression of the overall swirling airflow can be obtained from the 2D velocity distribution shown in Fig. 7 using particle image velocimetry (PIV) measurements. The PIV system consisted of a frequency-doubled, Nd: YAG laser, double shutter CCD camera and a sequencer. The airflow is seeded with alumina (Al2O3) of approximately 1- 10 µm size. A commercial PIV software (Lavision Davis 8.3) is used for the vector realizations by spatial cross-correlation of the particle images. The figure shows the 2D axial velocity distribution at an airflow rate Qair of 250 lpm (unpublished data). A converging-diverging flowfield is created at the exit of the burner due to a combination of the swirling flowfield and the presence of the bluffbody. The strong swirling flow, with the strength proportional to the swirling velocity, and the bluffbody effect creates a vortex breakdown downstream. Near to the burner exit where the bluffbody effects are stronger a toroidal vortex zone is created. Farther downstream from the nozzle the bluffbody effect wanes down and the flow subsequently diverges due to the effect of the swirl. The swirl effect becomes dominant creating a mild central recirculation zone. The velocity distributions shown are for test cases without any flow through the injector. So the image is used only for giving a qualitative impression about the swirling flowfield produced in this burner and variations in the flow-field are expected in presence of injector flow, especially in the bluffbody recirculation region. Such a convergent-divergent flow field influences the fuel droplet-air mixing and the orientation of the stoichiometric surface in the mixing region.

For the measurements with the co-flow of swirling airfield the injector was fixed at the center of the bluffbody of the burner. This poses a problem in capturing the spray pattern at the immediate exit of the injector as the injector sits approximately 11 mm behind the air nozzle exit (refer Fig. 4). So, this will hinder the visualization of the primary breakup process where the effect of injection velocity is felt. The secondary breakup on the other hand will be significantly affected by the relative velocity. Figure 8 shows an exemplary shadow-graph of the droplet pattern at the burner exit (11 mm downstream from the injector exit) with the swirling co-flow of air (MR = 36). It is seen that the fine droplets from the spray are distributed spatially at all investigated MR. High concentration of droplets is observed off-axis due to the swirling co-flow. Also, the co-swirling air tends

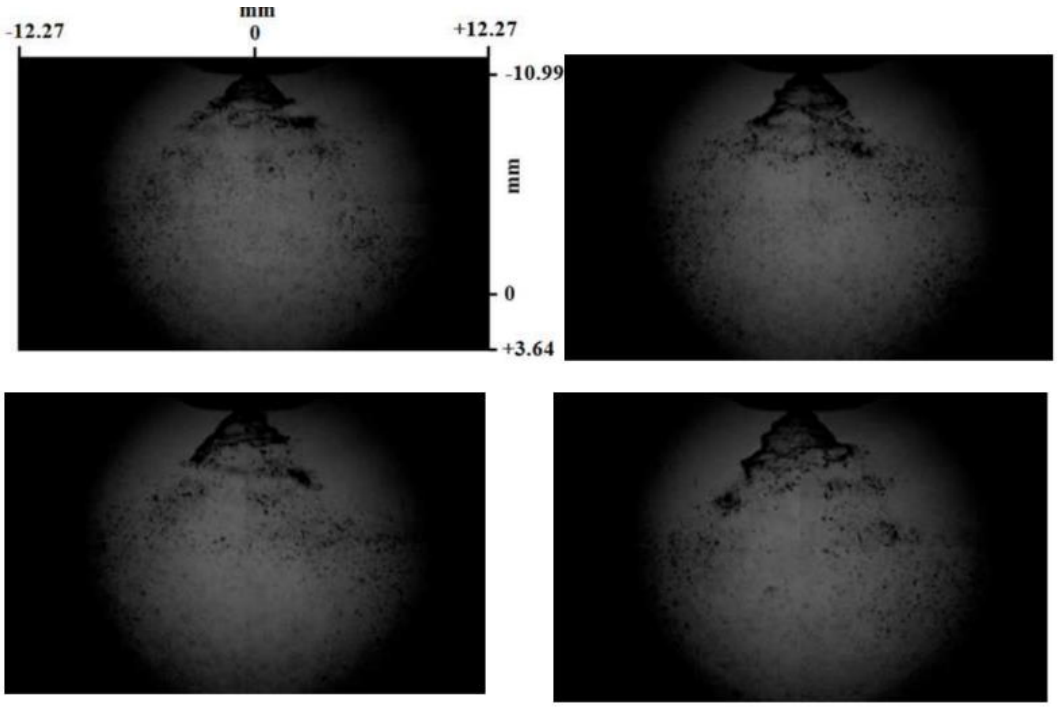

Fig. 5. Representative instantaneous shadowgraph images in the absence of co-swirling air flow.

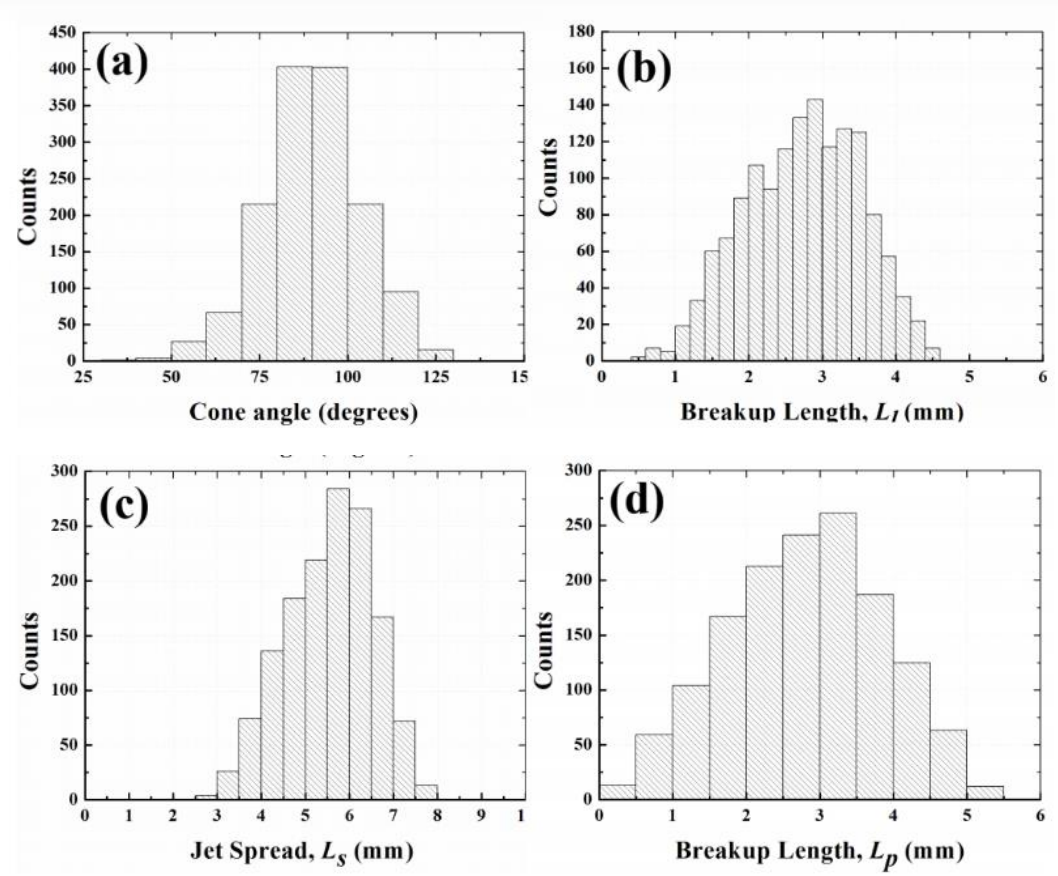

Fig. 6. Histogram of the spray parameters for the case without co-swirling air flow (a) Cone angle (b) End point based breakup length (L_l),(c) Jet spread (L_s) and, (d) Profile based breakup length (L_p).

to recirculate the droplets towards the centerline axis of the burner, because of the strong recirculation. Though it is not clearly visible in the shadowgraphy image, it was more evident from the PDPA measurements when comparing the time elapsed for measuring the 15000 droplet counts at various locations.

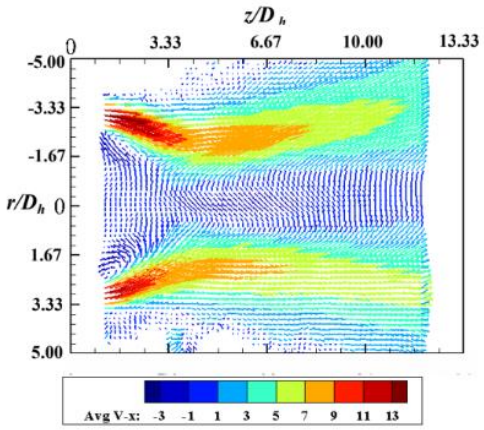

Fig. 7. Time averaged axial velocity distribution for an air flow rate of 250 lpm in the absence of flow through the injector (unpublished data).

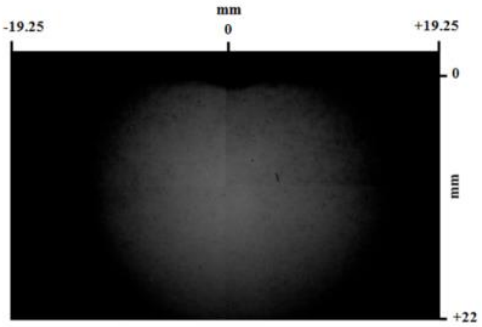

Fig. 8. Representative instantaneous shadowgraph image of the spray distribution in the presence of co-swirling air flow for MR = 36. When compared to the shadowgraph images shown in Fig. 5 the imaged area is 11 mm downstream from the injector exit.

4.2 Droplet Velocity and SMD Measurements

In the modeling of sprays in a combustion environment one of the most valuable parameter is the droplet velocity, as it provides information about the drag coefficients and trajectory angles. However, this is not straight forward to model in swirling flowfield due to the complex interaction between the droplets and the gas phases. So information about the spatial distribution of droplet velocity and diameter are valuable inputs for the modeling efforts.

4.2.1 Without Co-Swirling Airflow

Figure 9(a) shows the radial variation of normalized mean axial velocities (v/v_{max}) of the droplets without any co-swirling airflow at different planes downstream of the burner exit. Each ensemble consists of 40000 realizations and only a few of the downstream planes are shown for clarity. The mean axial velocities are observed to have a maximum value of 5.13 m/s and a minimum value of 0.68 m/s. At $z/D_h = 0.83$ downstream from the burner exit the maximum streamwise velocity v_{max} occurs at the axis then decreases to $0.3v_{max}$ at the outer boundary of the spray. At each cross-sectional planes downstream, the droplets exhibit a maximum value of velocity closer to the axis of the injector spray and a minimum value of the velocity at the periphery of the spray. This is particularly interesting as in a hollow cone spray one would expect the velocities to be maximum at the spray boundary and relatively lower velocities at regions closer to the axis. One possible explanation is that due to infrastructural limitations the injector was not operated at the rated pressure of 7 bar, but was operated at an injection pressure of 6 bar for these investigations. So the spray formed is not completely of hollow cone nature, but rather close to of solid cone nature. However, this does not affect the research objectives as the goal here is to investigate the impact of swirling flow on the droplet characteristics, irrespective of whether the droplet is formed from a hollow cone or a solid cone injector. The decay of the droplet velocities with downstream distance due to mixing with the ambient air is also evident from the plots. On comparison between the left and right side of the mean axial velocities, a mild asymmetry in the velocity distributions is visible. It was found that there is a difference in maximum velocity of 0.64 m/s between the left and right sides of the spray and it resulted in a variation in the SMD's also, as will be seen in the following sections.

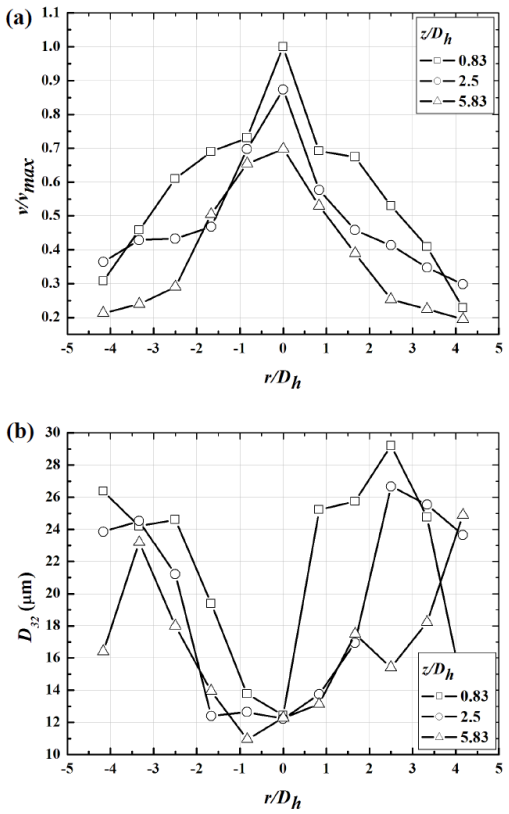

Fig. 9. Normalized mean axial velocity (a) and SMD (b) distribution at different axial planes in the absence of co-swirling air flow.

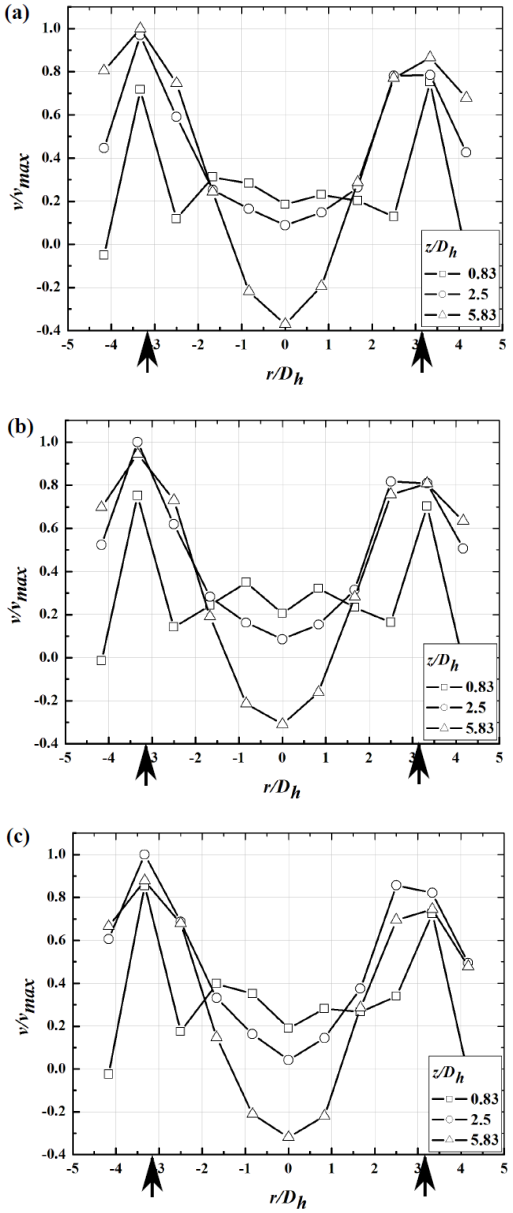

Fig. 10. Radial variation of normalized mean axial velocities of the droplet with co-swirled airflow at different axial planes for (a) MR = 36, (b) MR = 59 and, (c) MR = 116. The arrows mark the inlet location of the annular swirling airflow.

Figure 9(b) shows the radial variation of SMD with-out any co-swirled airflow at different planes down-stream to the burner exit. The droplet SMD varies from a minimum of 11.59 µm to a maximum of 29.71 µm. The bigger sized droplets are at the periphery of the spray and the smaller droplets are closer to the axis of the spray. This could be explained in conjunction with the velocity distribution. The high velocities seen closer to the axis lead to a faster disintegration of bigger droplets to smaller diameter droplets at these locations. Similarly, the relatively lower velocities at the periphery result in bigger droplet diameters. Also visible is the considerable asymmetry in the droplet SMD's. As mentioned before, this can be a direct effect of the asymmetry seen in the droplet axial velocity distributions. Overall the spray is distributed in such a way that smaller droplets with higher axial velocities crowd near to the burner centerline, and are surrounded by a cloud of larger droplets with low mean axial velocities.

4.2.2 With Co-Swirling Airflow

Figures 10(a)-(c) shows the radial distribution of mean axial velocities of the droplets in the presence of swirling flowfield. The droplet velocities at three downstream locations from the nozzle exit are plotted for three different MR = 36, 59 and 116. The three locations correspond to the bluffbody influenced region (z/Dh = 0.83), region close to the transition region (z /D_h = 2.5) and the swirl influenced region (z /D_h = 5.83). It is pretty clear that the droplet motion is now heavily influenced by the co-flowing air with the velocity pattern closely mimicking the flowfield witnessed in Fig. 7. A mild asymmetry between the left and right side of the image is also evident, arising from the asymmetry existing in the injector flow as seen before. The maximum velocity locations around $r/D_h \approx 3$ correspond to the high-velocity airflow inlet and farther away from the axis ($r/D_h > \pm 3$) the velocities decreases due to the mixing of the air jet with the atmosphere. The dip in the velocities close to the axis represents the reverse flow regions of the bluffbody and the swirl flow. Though the droplets close to the axis for $z/D_h = 0.83$ are located in the bluffbody recirculation regions in all the 3 cases it still maintains a positive axial velocity due to the high liquid jet velocity from the injector. How-ever as the droplet reaches the swirl influenced region (z/D_h = 5.83) the jet velocity is decayed to such an extent that the droplet is carried by the swirling flowfield. This results in a negative velocity closer to the axis. Consequently the recirculating droplet will have higher diameters than those at $z/D_h = 0.83$ plane due to the longer residence time, as will be seen in the SMD distributions later on. The maximum and minimum droplet axial velocities recorded at different planes for increasing MR are reported in Table. 2. With increasing MR there is a corresponding increase in the minimum and maximum velocity of the droplet at all z/D_h. For all MR the droplets achieve maximum velocity in the transition region. And the droplets with the minimum (negative) velocities are in the swirl influenced region closer to the axis. The magnitudes of which increases with increasing MR in the air in-flow region and decreasing in the centerline region due to a strengthening of the reverse flow.

Figure 11 shows a comparison of the mean axial velocities along the centerline with and with-out the co-swirling airflow for the three MR's investigated. The influence of the swirling flow-field on the droplet velocity is unmistakable. With-out the swirling flow the droplet velocities decay with downstream distance as expected. In the presence of swirling flow the droplets exhibit a positive velocity up to approximately $z/D_h = 2.5$, which is inside the bluffbody recirculation region. I.e., when compared to the 2D-PIV velocity distribution shown in Fig. 7

Table 2 Mean Axial Velocity v m/s

MR	z/D_h=0.83		z/D_h=2.5		z/D_h=5.83	
	Min	Max	Min	Max	Min	Max
36	-0.28	8.64	0.42	10.11	-3.22	8.88
59	-0.28	9.11	1.04	12.11	-3.74	11.43
116	-0.82	12.11	1.42	15.6	-5.95	16.09

Table 3 SMD (D_{32}) μm

MR	z/D_h=0.83		z/D_h=2.5		z/D_h=5.83	
	Min	Max	Min	Max	Min	Max
36	12.44	31.88	13.13	31.65	10.78	40.64
59	13.64	31.61	18.99	37.43	12.36	33.26
116	15.18	33.21	14.5	43.31	17.46	29.03

it is clear that droplets man-age to maintain a positive velocity in spite of the reverse flow existing in this region. As the injector spray velocity is more dominant than reverse flow velocities the droplets sustain a positive velocity. The high-velocity gradient also aids in the generation of droplets with smaller diameters in this region. This means that with increasing distance and a corresponding decrease in droplet velocity there will be an increase in the SMD. With in-creasing MR a small increase in the droplet velocity is visible, emphasizing the influence of convective flow velocity on the droplet velocity. The droplet flow reverses thereafter as it enters the recirculation zone of the swirl influenced region. Here, z/D_h = 2.5 - 3.3 approximately represents the transition region between the bluffbody and swirl influenced regions. The droplet velocities pick up again as it approaches the boundary of the recirculation region of the swirl influenced region. Similar to the bluff-body influenced region, the droplet reverse flow is also seen to strengthen with increasing MR.

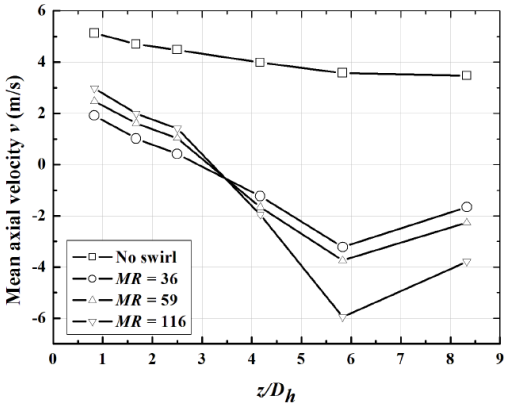

Fig. 11. Comparison of mean axial velocity of droplets along the burner axis at different axial locations with and without co-swirled air flow for (a) MR = 36, (b) MR = 59 and, (c) MR = 116.

The radial variation of droplet SMD in presence of co-swirled airflow for different MR's at different axial planes is shown in Fig 12. The corresponding minimum and maximum SMD values at various z/D_h locations are listed in Table. 3. The droplets exhibit a minimum value of SMD at locations closer to the exit of the burner. Also, the minimum droplet size is seen on one side of the injector tip, the reasons for which is not clear at present. This could be a result of the relatively high-velocity gradient that exists locally between the liquid jet and the surrounding gas (the location is closer to the inlet of the swirling airflow) that resulted in the breaking up of the droplet into finer sizes. The unusual shape of the SMD distribution can be explained by comparing it with the 2D PIV image is shown in Fig 7. For a fixed z/D_h the increase or decrease in SMD values more or less correlates with whether the droplet is in the high velocity region or the recirculation region respectively. Once the droplet enters a recirculation zone there is a high probability of droplet agglomeration as the residence times are longer, and thereby an increase in SMD. This is more evident in the Fig 13where the axial variation of SMD with and without the swirling flowfield is plotted. The presence of swirling flow in general lead to an increase in the SMD for all MR. The droplet SMD is greater in the swirl influenced recirculation zone than in the bluffbody region. The reasons for the abrupt peaks in the SMD plots (Fig 12(a), r/D_h=-2, z/D_h = 2.5 for example) is not clear yet. It is suspected to be due to the droplets agglomerating and dripping from the edges of the bluffbody during the long operation of the injector.

In reactive flow environment droplet evaporation involves simultaneous heat and mass transfer process and the overall rate of droplet evaporation depends on the droplet diameter and the velocity relative to the surrounding gas. The rates of heat and mass transfer is affected by the drop Reynolds number, which will vary throughout the droplet life time. It is evident from the results above that the

swirling flowfield can alter the spray/droplet characteristics of an injector and thereby the heat and mass transfer characteristics. This will have severe implications on flame stabilization and combustion efficiency. In general the droplets that follows the swirling gas movement are prone to droplet agglomeration owing to the longer residence time. Whereas those that are capable of breaking away from the high centrifuging of swirl due to the high droplet velocities result in a relatively smaller diameter droplets. Fine atomization produces high surface to volume ratio in the liquid phase thereby promoting rapid evaporation and high combustion rates. The fine droplets are also necessary for the rapid evaporation and easy ignition of the flame kernel in the start-up of an engine. In the investigated burner the fine droplets in the bluffbody influenced region of hot gases evaporate rapidly and the hot chemically active combustion species will be transported towards the root of the flame, thereby improving its stability. Due to the centrifugal forces resulting from the swirling motion the coarse droplets will be separated from the smaller droplets and evaporate later at the swirl influenced regions. The presence of strong recirculation seen in this region, both in PIV and in droplet velocity distribution, for all MR implies that the combustion at these locations will be less dependent on SMD due to the presence of the hot recirculating gases. The results presented above show that in the design of the injectors for practical applications, the investigations in the presence of the swirling flow-field are mandatory as the droplet generation mechanisms will be hugely influenced by the surrounding flow field.

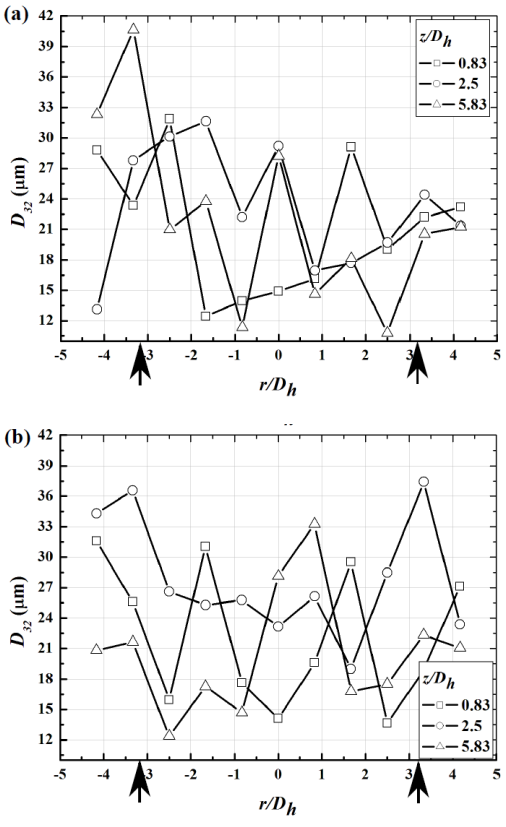

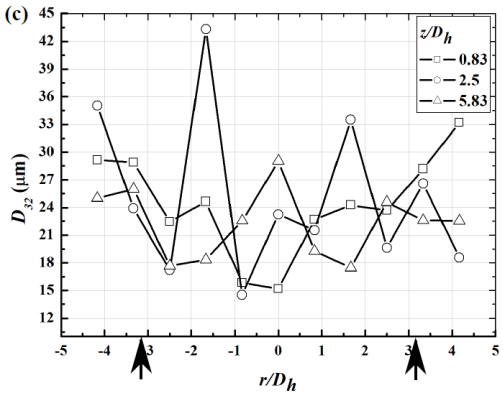

Fig. 12. Radial variation of SMD of droplets from the commercial injector with co-swirled air flow at different planes downstream from the burner exit (a) MR = 36, (b) MR = 59 and, (c) MR = 116. The arrows mark the inlet location of the annular swirling airflow.

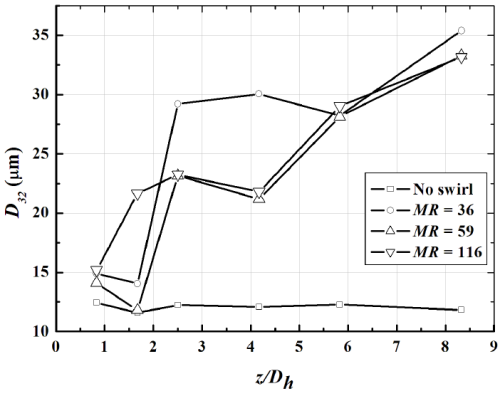

Fig. 13. Comparison of SMD of droplets at different axial locations along the burner axis with and without co-swirled air flow for (a) MR = 36, (b) MR = 59 and, (c) MR = 116.

5. CONCLUSIONS

An experimental investigation on the influence of swirling co-flow on the spray characteristics, droplet distribution, SMD and 1D velocity distribution under isothermal conditions is investigated in this study. Previous 2D-PIV measurements on the swirl flow generated in the investigated model burner has shown a convergent-divergent flowfield at the exit of the burner. The flowfield closer to the exit was influenced by the strong bluffbody effect creating the convergent field and farther down-stream in the diverging section the flow was influenced by the swirling effect. The injector mounted at the axis of the bluffbody produced spray characteristics typical of pressure swirl atomizer in the absence of swirling co-flow. However in the presence of swirling co-flow, with varying air-liquid momentum flux ratios, the influence of the swirl flow was unmistakable. Though the droplets maintained a positive velocity closer to the bluffbody, the droplets are affected by the flow recirculation at downstream locations. The velocity profiles of the droplets more or less mimicked the 2D velocity distribution of the swirl flow. For all the investigated momentum flux ratios

the droplet diameter was higher than those without the swirling co-flow. At each axial plane finer droplets were formed at regions closer to the high-velocity air inflow regions and coarser droplets at regions closer to the recirculation zones. Droplet coagulation is expected in the recirculation zones owing to the longer residence times in these regions. This will have serious implications in reactive flow environment as the spatial evolution of the ignitable fuel/air mixture is related to the droplet atomization and evaporation process. These studies highlight the need for understanding the mechanisms involved in the atomization pro-cess in the presence of surrounding flowfield. Such information is valuable for the design engineers in aero gas turbine and liquid propellant rocket engine industries.

ACKNOWLEDGMENTS

The authors express sincere gratitude to Dr. Prathap and Dr. Aravind for the support and facilities provided for this study. The authors also wish to acknowledge the support from the technical staff of Aerospace department in the development of the burner.

REFERENCES

Aliseda, A., E. Hopfinger, J. Lasheras, D. Kremer, A. Berchielli, and E. Connolly (2008). Atomization of viscous and non-newtonian liquids by a coaxial, high-speed gas jet. experiments and droplet size modeling. *International Journal of Multiphase Flow* 34, 161–175.

Charalampous, G., C. Hadjiyiannis, and Y. Hardalupas (2019). Proper orthogonal decomposition of primary breakup and spray in co-axial airblast atomizers. *Physics of Fluids* 31, 043304.

de la Rosa, A. (1992). The effect of swirl on the velocity and turbulence fields of a liquid spray. *Journal of Engineering for Gas Tur-bines and Power* 114, 72–81.

Faeth, G. (1983). Evaporation and combustion of sprays. *Progress in Energy and Combustion Science* 9, 1–76.

Fan, Y., N. Hashimoto, H. Nishida, and Y. Ozawa (2014). Spray characterization of an air-assist pressure-swirl atomizer injecting high-viscosity jatropha oils. *Fuel* 121, 271–283.

Glassman, I. and R. A. Yetter (2008). *Combustion*. New York: Academic Press.

Hadef, R. and B. Lenze (2005). Measurements of droplets characteristics in a swirl-stabilized spray flame. *Experimental Thermal and Fluid Science* 30, 117–130.

Jarpala, R., N. Burle, M. Voleti, and R. Sadanandan (2017). Effect of swirl on the flame dynamics and pollutant emissions in an ultra-lean non-premixed model gt burner. *Combustion Science and Technology* 189(10), 1832–1848.

Kumar, A. and S. Sahu (2018). Liquid jet breakup unsteadiness in a coaxial air-blast atomizer. *International Journal of Spray and Combustion Dynamics* 10(3), 211–230.

Lasheras, J. C., E. Villermaux, and E. J. Hopfinger (1998). Break-up and atomization of a round water jet by a high-speed annular air jet. *Journal of Fluid Mechanics* 357, 351–379.

Lefebvre, A. (1989). *Atomization and Sprays*. New York: Taylor and Francis.

Lefebvre, A. (1998). *Gas Turbine Combustion*. New York: Taylor and Francis

Lian, Z. and S. Lin (1990). Breakup of a liquid jet in swirling gas. *Physics of Fluids* 2, 2134–2139.

Liao, Y., S. Jeng, M. Jog, and M. Benjamin (2000). The effect of air swirl profile on the instability of a viscous liquid jet. *Journal of Fluid Mechanics* 424, 1–20.

Marchione, T., A. Amoresano, and F. Beretta (2007). Experimental investigation of a pressure swirl atomizer spray. *Journal of Propulsion and Power* 23(5), 1096–1101.

Matas, J.-P., A. Delon, and A. Cartellier (2018). Shear instability of an axisymmetric airwater coaxial jet. *Journal of Fluid Mechanics* 843,575600.

Mohammed, S., N. Gupta, D. Mishra, and R. Sadanandan (2019, March). Application of digital image processing method for spray characterization. *In 6th International Conference on Signal Processing and Integrated Networks*, Delhi, India.

Rajamanickam, K. and S. Basu (2017). Insights into the dynamics of spray-swirl interactions. *Journal of Fluid Mechanics* 810, 82–126.

Rink, K. and A. Lefebvre (1986). Influence of fuel drop size and combustor operating conditions on pollutant emissions. *SAE Technical Paper* 861541.

Rizk, N. and A. Lefebvre (1985). Internal flow characterisitics of simplex swirl atomizers. *Journal of Propulsion and Power* 1, 193–199.

Sadanandan, R. (2015). Ultra lean non-premixed gaseous fuel burner. Indian Patent Application. No: 6632/CHE/2015.

Varga, C. M., J. C. Lasheras, and E. J. Hopfinger (2003). Initial breakup of a small-diameter liquid jet by a high-speed gas stream. *Journal of Fluid Mechanics* 497, 405–434.

Wang, X. and A. Lefebvre (1987). Mean drop sizes from pressure-swirl nozzles. *Journal of Propulsion and Power* 3, 11–18.

Yao, S., J. Zhang, and T.J.Fang (2012). Effect of viscosities on structure and instability of sprays from a swirl atomizer. *Experimental Thermal and Fluid Science* 39, 158–166.